ORGANOMETALLICS

pubs.acs.org/Organometallics Article

Z-Selective Monothiolate Ruthenium Indenylidene Olefin Metathesis Catalysts

Wietse Smit, Jonas B. Ekeli, Giovanni Occhipinti,* Bartosz Woźniak, Karl W. Törnroos, and Vidar R. Jensen*

Cite This: https://dx.doi.org/10.1021/acs.organomet.9b00641 Read Online

ACCESS | Metrics & More | Article Recommendations | Supporting Information

ABSTRACT: Ru-alkylidenes bearing sterically demanding arylthiolate ligands (SAr) constitute one of only two classes of catalyst that are *Z*-selective in metathesis of 1-alkenes. Of particular interest are complexes bearing pyridine as a stabilizing donor ligand, [RuCl(SAr)(=CHR)(NHC)(py)] (R = phenyl or 2-thienyl, NHC = *N*-heterocyclic carbene, py = pyridine), which initiate catalysis rapidly and give appreciable yields combined with moderate to high *Z*-selectivity within minutes at room temperature. Here, we extend this chemistry by synthesizing and testing the first two such complexes (**5a** and **5b**) bearing 3-phenylindenylidene, a ligand known to promote stability in other ruthenium-based olefin metathesis catalysts. The steric pressure resulting from the three bulky ligands (the NHC, the arylthiolate, and the indenylidene) forces the thiolate ligand to position itself *trans* to the NHC ligand, a configuration different from that of the corresponding alkylidenes. Surprisingly, although this configuration is incompatible with *Z*-selectivity and slows down pyridine dissociation, the two new complexes initiate readily at room temperature. Although their thermal stability is lower than that of typical indenylidene-bearing catalysts, **5a** and **5b** are fairly stable in catalysis (TONs up to 2200) and offer up to ca. 80% of the *Z*-isomer in prototypical metathesis homocoupling reactions. Density functional theory (DFT) calculations confirm the energetic cost of dissociating pyridine from **5a** (= **M1-Py**) to generate 14-electron complex **M1**. Whereas the latter isomer does not give a metathesis-potent allylbenzene π-complex, it may isomerize to **M1-trans** and **M2**, which both form π-complexes in which the olefin is correctly oriented for cycloaddition. The olefin orientation in these complexes is also indicative of *Z*-selectivity.

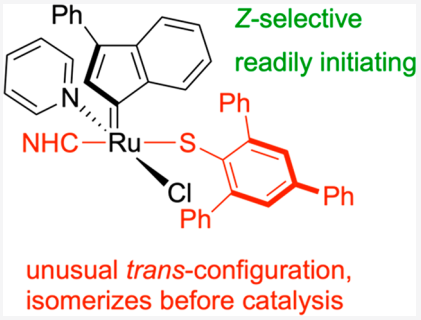

INTRODUCTION

Olefin metathesis (OM) is the most versatile catalytic method for carbon−carbon double-bond formation. Several well-defined olefin metathesis catalysts have been developed, based on molybdenum, tungsten, or ruthenium.[1−8] In general, ruthenium-based catalysts are the most robust against oxygen, moisture, and substrates with heteroatom-containing functional groups.[9] Grubbs first-generation catalyst (**1a**, Chart 1) as well as the more stable and active second-generation catalyst, **1c**, are both frequently used in a variety of OM reactions.

Nevertheless, challenges in Ru-catalyzed olefin metathesis still remain. For example, these catalysts do not mediate ring-closing metathesis (RCM) reactions that form tetrasubstituted cyclic alkenes, and already trisubstituted alkenes are difficult to obtain via RCM.[10] Furthermore, the temperature-stability of **1a**, and to some extent also **1c**, is limited, reducing their applicability in reactions that require high temperatures.[11] In addition, synthesis of **1a−c** requires costly and dangerous chemicals such as diazoalkane derivatives.

The above challenges have motivated the investigation of alternatives to the traditional alkylidene ligands.[10] Reaction of $[RuCl_2(PPh_3)_3]$ with the cheap and easily available 1,1-diphenylpropargyl alcohol was believed to have given the

Chart 1. Ru-Based Olefin Metathesis Catalysts

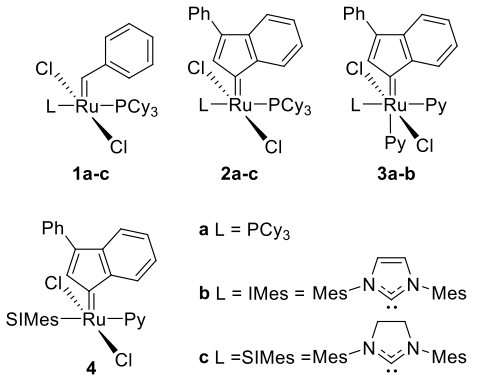

Cy = cyclohexyl, Mes = mesityl, Py = pyridine

Received: September 24, 2019

diphenylallenylidene complex [$RuCl_2$(=C=C=CPh_2)(PPh_3)$_2$].[12] However, X-ray crystallographic analysis and a review of previously recorded spectroscopic data later showed that a rearrangement had taken place, to a cyclized vinyl carbene or indenylidene complex.[11,13] Subsequently, substitution of PPh_3 with PCy_3 and various *N*-heterocyclic carbenes (NHC) led to a family of indenylidene-bearing ruthenium complexes, corresponding to both first- (**2a**) and second-generation (**2b**,**c**) Grubbs catalysts.[11,13−16] Consistent with the intention behind the alkylidene replacement, **2a** and **2c** are thermally much more stable than their benzylidene analogues, with no signs of decomposition even after 10 days of heating at 80 °C in toluene-d_8.[11] Catalysts **2a**−**c** performed well in RCM[14,17,18] and in the synthesis of complex natural products.[13,15,19−24] In addition, **2c** mediates RCM leading to tetrasubstituted cyclic alkenes.[10,17] However, the catalytic activities of **2a**−**c** are, in general, not higher than those of **1a**−**c**.

Major improvements in catalytic activity, in particular in the initiation and early phase of the metathesis experiments, have been obtained by substituting the remaining phosphine ligand in **1b** with two pyridine ligands.[25] Starting from **2a**−**c**, the same strategy has offered complexes **3a**,**b**[26,27] and **4**,[28] respectively. Although these mono- (**4**) and bis-pyridine (**3a**,**b**) complexes initiate catalysis faster, they also deactivate faster, with catalytic activity typically ceasing well before full conversion has been reached.[27]

The advantages of fast initiation are striking in *Z*-selective olefin metathesis. The ruthenium monothiolate congeners of Grubbs third-generation catalysts, a class of catalyst originally stabilized exclusively via benzylidene ether ligands,[29−32] not only initiate faster, but these pyridine-coordinated ruthenium monothiolate catalysts are also less inclined to isomerize the substrate and thus are more selective for metathesis than their counterparts bearing benzylidene ether ligands.[33,34]

Thus, even if the monothiolate catalysts are less *Z*-selective than Grubbs's cyclometalated catalysts[35−38] and higher *Z*-selectivities can also be reached when using *Z*-configured substrates or cosubstrates in conjunction with Hoveyda's stereoretentive catechothiolate-coordinated catalysts,[39−41] they do have attractive catalytic properties: The pyridine-coordinated monothiolate catalysts can reach appreciable yields combined with moderate to high *Z*-selectivity within minutes in prototypical metathesis reactions of terminal olefins at room temperature. These catalysts can also be used in *Z*-selective metathesis of difficult substrates, such as dienes to form macrocyclic rings and ω-alkenoic acids to form α,ω-dicarboxylic acid alkenes.

Summarizing, the ruthenium monothiolate catalyst design is flexible, and even allows for immobilization of the catalyst by tethering the catalyst to a silica support via the thiolate.[32] Most importantly, *Z*-selective monothiolate analogues of first-, second-, and third-generation Grubbs-type catalysts exist. The main reason for this flexibility is that these *Z*-selective catalysts share key structural and mechanistic features with the Grubbs catalysts: they bind the reacting olefins and form the ruthenacyclobutane intermediate *trans* to the donor ligand (L in Chart 1).[31,42]

These similarities suggest that another structural facet found among the ruthenium dichloride metathesis catalysts, the Ru-indenylidene architecture, might also be transferred to the ruthenium monothiolate framework. If so, then the attractive properties of the indenylidene catalysts, such as improved temperature stability (see above), might be exploited in *Z*-selective catalysis. However, both the indenylidene and selectivity-inducing thiolate are sterically demanding ligands. Replacing a chloride ligand in **2b**−**c** with a bulky, selectivity-inducing arylthiolate would probably not be possible. Instead, complexes **3b** and **4**, the latter being commercially available, are more promising starting points for this substitution. Presumably, at least one pyridine ligand would readily dissociate to make room for the incoming thiolate, and a pyridine ligand might fit next to the thiolate aryl group in the catalyst precursor.

To test this hypothesis, we have pursued the synthesis of monothiolate analogues of NHC-coordinated ruthenium indenylidene complexes, with the goal to obtain *Z*-selective metathesis catalysts with attractive properties inherited in particular from the indenylidene ligand.

RESULTS AND DISCUSSION

Treatment of [$RuCl_2$(IMes)$(py)_2$(3-phenylindenylidene)] (**3b**), which was first prepared according to known procedures,[27] with 1 equiv of potassium 2,4,6-triphenyl-benzenethiolate in tetrahydrofuran (THF) readily led to compound **5a** (Scheme 1). Diffusion of *n*-pentane into a concentrated solution

Scheme 1. Synthesis of Compound 5a

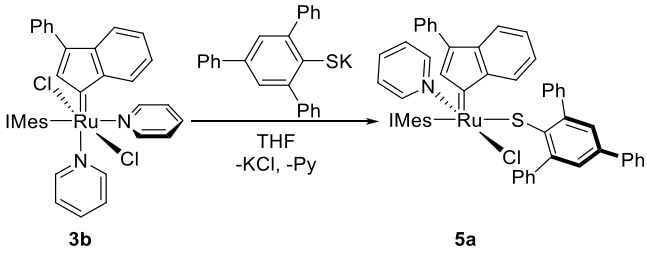

3b **5a**

of **5a** in dichloromethane (DCM) at low temperature (−32 °C) gave dark red crystals suitable for X-ray crystallographic analysis. The molecular structure, relevant bond lengths, and angles are shown in Figure 1.

Compound **5a** adopts a slightly distorted square pyramidal geometry, with the indenylidene occupying the apical position, a configuration typical of pentacoordinate Grubbs catalyst precursors. Surprisingly, however, in the basal plane, the two ligands with the strongest *trans* influence, the thiolate ligand (S1) and IMes (C1) are positioned *trans* to each other (C1−Ru1−S1 = 146°). The total steric pressure, larger than usual due to the indenylidene ligand, prevents the *cis*-coordination of the thiolate and the NHC observed in corresponding alkylidene monothiolate complexes.[29−31,33] Instead, in **5a**, the two anionic ligands are positioned *cis* to each other. While this *cis*-configuration of the anionic ligands has not been observed in other monothiolate-coordinated ruthenium-based olefin metathesis catalysts, this isomer is not uncommon among other ruthenium-based olefin metathesis catalysts.[43] Presumably, during the synthesis, pyridine dissociates to make room for the incoming bulky thiolate, followed by recoordination of pyridine *cis* to IMes. This unusual configuration, if maintained during catalysis, is not expected to be suitable for fast-initiating and *Z*-selective metathesis. First, with its position *trans* to chloride (Cl1), a ligand of little *trans* influence, pyridine is not guaranteed to dissociate rapidly. When it eventually dissociates, the incoming olefin and the ruthenacyclobutane (RCB) intermediate are expected to experience a roughly equally distributed steric pressure from the *trans*-positioned IMes and the thiolate, as opposed to selectivity-inducing steric pressure

https://dx.doi.org/10.1021/acs.organomet.9b00641
Organometallics XXXX, XXX, XXX−XXX

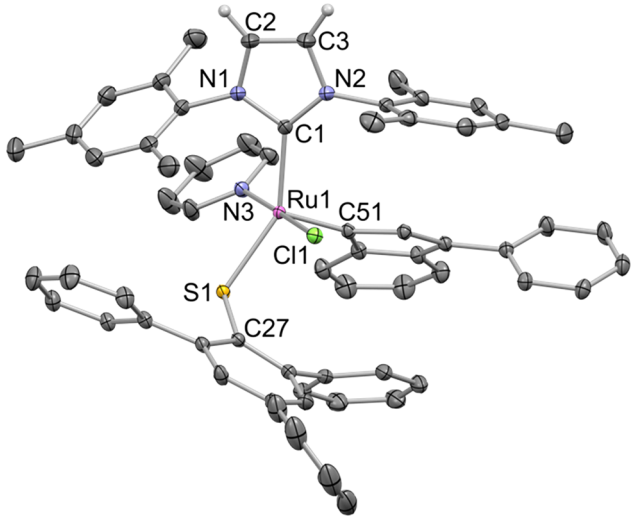

Figure 1. X-ray structure of **5a** with displacement ellipsoids drawn at the 50% probability level. Except for the NHC backbone (C2 and C3), hydrogen atoms and solvent molecules (DCM) are omitted for clarity. Selected geometric parameters: Ru1−C1 = 2.0911(16) Å, Ru1−Cl1 = 2.3903(4) Å, Ru1−N3 = 2.1113(14) Å, Ru1−C51 = 1.8731(16) Å, Ru1−S1 = 2.3066(4) Å, C2−C3 = 1.346(3) Å; N1−C1−N2 = 103.24(14)°, C1−Ru1−Cl1 = 88.52(5)°, C1−Ru1−N3 = 89.71(6)°, C1−Ru1−C51 = 106.20(7)°, C1−Ru1−S1 = 145.78(5)°, C51−Ru1−Cl1 = 91.76(5)°, C51−Ru1−N3 = 93.03(6)°, C51−Ru1−S1 = 108.01(5)°, N3−Ru1−S1 = 88.53(4)°, Cl1−Ru1−S1 = 90.408(14)°, Ru1−S1−C27 = 114.26(5)°.

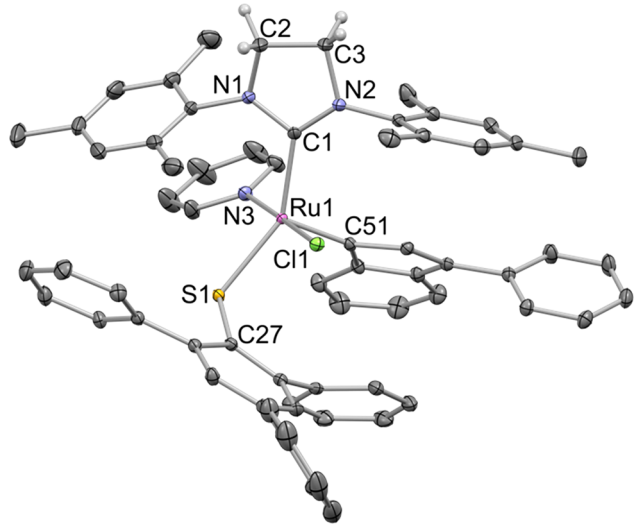

Figure 2. X-ray structure of **5b** with displacement ellipsoids drawn at the 50% probability level. Except for the NHC backbone (C2 and C3), hydrogen atoms and solvent molecules (DCM) are omitted for clarity. Selected geometric parameters: Ru1−C1 = 2.0795(15) Å, Ru1−Cl1 = 2.3879(4) Å, Ru1−N3 = 2.1134(14) Å, Ru1−C51 = 1.8745(15) Å, Ru1−S1 = 2.3181(4) Å, C2−C3 = 1.520(2) Å; N1−C1−N2 = 106.56(14)°, C1−Ru1−Cl1 = 87.21(4)°, C1−Ru1−N3 = 91.37(6)°, C1−Ru1−C51 = 107.23(6)°, C1−Ru1−S1 = 145.07(4)°, C51−Ru1−Cl1 = 91.25(5)°, C51−Ru1−N3 = 93.03(6)°, C51−Ru1−S1 = 107.66(5)°, N3−Ru1−S1 = 88.48(4)°, Cl1−Ru1−S1 = 90.385(13)°, Ru1−S1−C27 = 113.73(5)°.

toward a single face of the RCB in known *Z*-selective monothiolate catalysts.[31]

The corresponding SIMes-bearing compound, **5b** (Scheme 2), was obtained by reacting [$RuCl_2$(SIMes)(py)(3-phenyl-indenylidene)] (**4**), commercially available as Umicore M31, with 1 equiv of potassium 2,4,6-triphenyl-benzenethiolate in THF. Unfortunately, we could not reach conversions above 70%. Extension of the reaction time beyond 30 min and addition of more thiolate led to massive product decomposition. Purified **5b** was obtained by filtering the reaction mixture, dissolving the residue in DCM, and precipitating or crystallizing using mixtures of DCM and *n*-pentane at low temperature (−32 °C). Attempts at synthesizing analogues of **5a**,**b** by using an even more sterically demanding thiolate, potassium 2,4,6-tri(di-*m*-methylphenyl)benzenethiolate, resulted in either decomposition or yields that were too low to allow for product isolation.

Scheme 2. Synthesis of Compound 5b

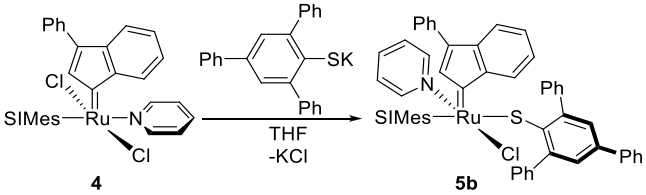

Diffusion of *n*-pentane into a concentrated solution of **5b** in DCM at low temperature (−32 °C) yielded dark red crystals suitable for X-ray crystallographic analysis. The molecular structure, relevant bond lengths, and angles are shown in Figure 2.

The crystals of **5a** and **5b** are isomorphous, that is, they belong to the same space group $P\bar{1}$ and have almost identical cell parameters (see Table S1). The packing effects should thus be very similar for the two compounds and allow for meaningful comparison of structural parameters. This is a welcome opportunity to gauge the effect of the two different NHC ligands, IMes and SIMes, in **5a** and **5b**. The electronic and steric effects of these two ligands are still a matter of debate.[44−48]

As in **5a**, compound **5b** adopts a slightly distorted square pyramidal geometry, with the indenylidene occupying the apical position and with *trans*-positioning of the SIMes and the thiolate in the basal plane. The Ru−C(NHC) bond is slightly shorter in **5b** than in **5a** (Ru1−C1 = 2.079 vs Ru1−C1 = 2.091 Å), indicating that SIMes is more strongly bound to ruthenium than IMes. This is consistent with the slightly stronger L → Ru σ-donation and $d_\pi \rightarrow L_\pi$ back-donation calculated using density functional theory (DFT), for SIMes compared to IMes.[44] Furthermore, the N1−C1−N2 angle is wider in **5b** (107°) than in **5a** (103°). The wider N1−C1−N2 angle and shorter Ru−C(NHC) bond in **5b** imply higher steric pressure from the mesityl groups on neighboring ligands. This, together with the stronger L → Ru σ-donation should translate into longer bond distances to ruthenium for the other ligands. Indeed, this holds true for the covalent and dative metal−ligand bonds. The Ru═C(ind) and Ru−N(py) bonds are slightly longer in **5b** (1.875 and 2.113 Å, respectively) than in **5a** (1.873 and 2.111 Å), whereas the effect is more pronounced for the Ru−S bond *trans* to the NHC, which is more than 1 pm longer in **5b** than in **5a**. In contrast, the ionic Ru−Cl bond appears to adapt to the overall arrangement of the other ligands and is 0.2 pm *shorter* in **5b** than in **5a**. Similar results are obtained when the DFT-optimized geometries of **5a** and **5b** are compared, again confirming that in this particular case packing effects are not overriding the electronic and steric differences between IMes and SIMes; see the Supporting Information for details.

https://dx.doi.org/10.1021/acs.organomet.9b00641
Organometallics XXXX, XXX, XXX−XXX

As shown by the complexity of the ^{1}H and ^{13}C NMR spectra (see the Supporting Information), the pyridine ligand in both **5a** and **5b** dissociates to give mixtures of **5a** and **5b** and the corresponding pyridine-free ruthenium complexes. These complexes have *trans*-configured anionic ligands, as discussed in the "Molecular-Level Calculations" subsection below.

The ease with which pyridine dissociates from **5a** and **5b** is surprising given the *trans*-position of this ligand relative to chlorine. To help understand the unexpected lability of pyridine, variable-temperature ^{1}H NMR experiments of complex **5a** in $CDCl_3$ were conducted; see the "Variable-Temperature ^{1}H NMR Experiments on **5a**" section in the Supporting Information for details. The free pyridine was identified by the two multiplets at 8.62 (CH (2,6)) and 7.68 ppm (CH (4)), while the third multiplet at 7.29 ppm (CH (3,5)) was in part masked by other aromatic peaks. These experiments reveal that pyridine dissociation from **5a** is spontaneous, albeit relatively slow, at room temperature. Whereas the rate of dissociation is much slower than for the closely related alkylidene-based catalysts,[33] the equilibrium is shifted more to the right: The degree of pyridine dissociation is estimated to reach ca. 80% (see the Supporting Information), compared to up to 32% for the alkylidene-based catalysts.[33] Still, equilibrium is not reached instantaneously, and dissociation is associated with a non-negligible barrier (see the estimate in the computational section below). The reverse reaction is even slower since the equilibrium is firmly shifted to the right.

Surprisingly, the variable-temperature NMR experiments also reveal that **5a** and **5b** are much less thermally stable than other indenylidene-bearing catalysts such as **2a−c** and **3a−c**. Decomposition products were detected within minutes when the sample was heated to 313 K or above. These are much lower temperatures than those tolerated by alkylidene-bearing analogues,[33] suggesting that the poor thermal stability of **5a** and **5b** is caused by the steric congestion resulting from the combination of the indenylidene with two other sterically demanding ligands, the thiolate and the NHC. Very little of the additional steric congestion in these thiolate-coordinated complexes compared to the corresponding dichlorides is due to sulfur itself; see the "Molecular-Level Calculations" section below.

Catalytic Results. As already noted, **5a** and **5b** are prone to lose the pyridine ligand. This dissociation creates a vacant coordination site. As expected from this unsaturation, both complexes readily initiate metathesis at room temperature (see Table 1), at a rate much faster than that of the 2-isopropoxybenzylidene congeners.[29,30] Still, in accordance with the already noted barrier to pyridine dissociation, the initiation rate of the indenylidene catalysts is clearly lower than that of the closely related pyridine-coordinated alkylidene counterparts.[33] Interestingly, the indenylidene catalysts offer *Z*-selectivities up to and above 80% in standard metathesis homocoupling of 1-alkenes, even though the two potentially selectivity-inducing bulky ligands, the NHC and the arylthiolate, are positioned *trans* to each other in the pyridine-stabilized precursors **5a** and **5b**. This result strongly suggests that a *cis*−*trans* isomerization of the anionic ligands[49] occurs during the initiation of these catalysts. Similar to the 2-isopropoxybenzylidene congeners,[50] SIMes-coordinated catalyst **5b** is more active and *Z*-selective, albeit with lowering of the selectivity at higher conversions (entry 5). Relatively little double-bond isomerization of the substrate is observed with **5b**, in particular with allylbenzene (entries 5 and 6) and 1-octene (entry 9).

Table 1. Homocoupling of Neat Substrates at RT

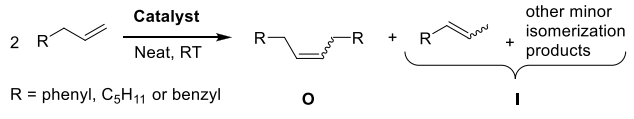

run	cat.	cat. load (mol %)	sub.[a]	time (min)	conv. (%)[b]	O/I[b]	Z (%)[b]
1	**5a**[c]	0.5	AB	5	8	13	80
2	**5a**[c]	0.5	PB	5	14	3	82
3	**5a**[c]	0.5	PB	15	34	4	82
4	**5a**[c]	0.1	OCT	15	4	9	85
5	**5b**	0.5	AB	5	55	62	76
6	**5b**[d]	0.5	AB	30	19	28	83
7	**5b**	0.5	PB	15	34	8	88
8	**5b**	0.5	PB	60	72	4	83
9	**5b**	0.1	OCT	15	5	36	87
10	**5b**	0.01	OCT	240	22	10	84
11	**3b**	0.5	AB	5	59	43	16
12	**4**	0.5	AB	5	80	59	16

[a]AB = allylbenzene, PB = 4-phenyl-1-butene, OCT = 1-octene. [b]Determined by ^{1}H NMR using hexamethylbenzene as internal standard. [c]Freshly crystallized **5a** (batch B; see Table 2 and associated discussion) + 0.1 equiv of pyridine. [d]Additive: 0.1 equiv of pyridine.

However, with 4-phenyl-1-butene, and especially at high conversion (entry 8), double-bond migration becomes significant. To gauge the effects of the thiolate ligand, tests of the dichloride precursors (**3b** and **4**, respectively; see Schemes 1 and 2) for the synthesis of **5a** and **5b** in metathesis of allylbenzene have also been included (entries 11 and 12). A comparison between entries 1 and 11 (IMes-based catalysts) and 5 and 12 (SIMes-based), respectively, illustrates the dramatic effect on the Z-selectivity, which increases from 16% to above 75%, on exchanging a chloride for a thiolate. However, the increased *Z*-selectivity comes at the price of lower productivity, especially for **5a**, which also promotes more olefin isomerization than parent dichloride precursor **3b**.

Whereas **5b** loses much of its catalytic activity and selectivity for olefin metathesis on addition of pyridine (entry 6), the opposite is true for **5a**. Loss of pyridine from microcrystalline **5a** reduces the selectivity for both metathesis and the *Z*-isomer product. The reason is that, in contrast to **5b**, freshly crystallized **5a** contains slightly less than one equivalent of pyridine and even more pyridine is lost on recrystallization. Whereas the effect of pyridine on catalysis using **5a** is investigated explicitly below, in Table 2 and the associated discussion, the catalytic tests of **5a** reported in Table 1 were performed in the presence of 0.1 equiv of pyridine to ensure reproducibility between different batches of **5a**. As indicated above, **5a** contains less than one equivalent of pyridine. For example, a recrystallized batch of **5a** (batch A), was determined (by ^{1}H NMR; see the Supporting Information) to contain 0.92 equiv of pyridine, while a freshly crystallized batch (batch B) contained 0.96 equiv. This suggests that the loss of pyridine originates from cocrystallization of **5a** with the *trans*-configured pyridine-free species (see the "Molecular-Level Calculations" section below) resulting from dissociation of pyridine from **5a** in solution. The latter dissociation is irreversible; see the Supporting Information for experimental results and the computational analysis below. In contrast, no pyridine was lost when the first crystallized material (batch B) was dried under vacuum.

Surprisingly, despite the minor loss of pyridine (0.04 equiv) on recrystallization, batch A is much less *Z*-selective than batch

https://dx.doi.org/10.1021/acs.organomet.9b00641
Organometallics XXXX, XXX, XXX−XXX

Table 2. Catalysis Using 0.5 mol % 5a: Influence of Pyridine

run	batch[a]	pyridine (equiv)	time (min)	conv. (%)[b]	O/I[b]	Z (%)[b]
1	A	0	5	14	10	61
2	A	0	15	24	7	40
3	A	0.1	5	5	14	82
4	A	0.1	15	12	11	80
5	A	0.1	60	28	12	71
6	A	0.1	120	62	8	46
7	A	0.2	5	2	5	83
8	A	0.2	15	10	6	81
9	A	0.2	60	24	13	78
10	A	0.2	120	38	11	75
11	A	1	5	0.2	ND	ND
12	A	1	15	1	3	82
13	A	1	60	6	12	80
14	B	0	5	12	6	72
15	B	0	15	23	7	58
16	B	0.1	5	8	13	80
17	B	0.1	15	18	17	78
18	B	0.1	60	32	11	71
19	B	0.1	120	44	9	69

[a]The content of pyridine in batches A and B was determined by ^{1}H NMR to be 0.08 and 0.04 equiv lower than the stoichiometric amount. [b]Determined by ^{1}H NMR using hexamethylbenzene as internal standard.

B (Table 2: cf. entries 1−2 and 14−15). Remarkably, the *Z*-selectivity and the selectivity for olefin metathesis of batch A are improved on addition of 0.1 equiv of pyridine to the reaction mixture. The pyridine addition thus makes the catalytic performance of the two batches become similar (entries 3−6 and 16−19), albeit at the expense of reducing the catalytic activity of batch A. Addition of more than 0.1 equiv of pyridine reduces the initiation rate significantly and does not improve the *Z*-selectivity any further (entries 7−13).

The most likely cause for the drop in *Z*-selectivity following loss of pyridine is catalyst decomposition to isomerization-active ruthenium complexes. Indeed, the benefit of excess pyridine is more pronounced at higher conversion and at longer reaction time. The complexes resulting from loss of pyridine are much less stable than the 16-electron catalyst precursors, and ruthenium metathesis catalysts are known to decompose to species catalyzing double-bond migration in the substrate. This double-bond migration is most likely accompanied by *Z*−*E* isomerization of the product,[30] either catalyzed by the same species or, more likely (see below), by related metathesis catalyst decomposition products. The isomerization-active species, such as the 12-electron $RuCl_2(SIMes)$,[51] tend to be coordinatively less saturated than metathesis catalysts. Thus, although addition of pyridine reduces the catalytic activity for both metathesis and isomerization, the low-coordinate isomerization catalysts are deactivated more easily than the metathesis catalysts. Moreover, the *Z*−*E* alkene isomerization catalysts seem to be more easily deactivated than the double-bond migration catalysts.

Molecular-Level Calculations. As detailed above, the ligand arrangement in **5a** and **5b** is neither expected to lead to rapid initiation, nor to *Z*-selective metathesis. The initial pyridine dissociation from **5a** and the subsequent rearrangement into isomers expected to be *Z*-selective were thus investigated using DFT. Solvent effects of toluene, mimicking the catalytic experiments in the neat, largely apolar substrates, and chloroform, mimicking the above-described variable-temperature NMR experiments in $CDCl_3$, were included using a continuum solvent model as described in the Supporting Information. Whereas relative free energies are reported for the catalyst concentration used in the variable-temperature NMR experiments (1.86 mM in $CDCl_3$), the free energies discussed in the following are also, unless otherwise stated, the ones obtained for a standard state corresponding to a 1 M solution at room temperature.

The calculations first confirmed that pyridine dissociation is energetically costly. From **M1-Py**, the DFT model of **5a**, dissociation leads to a kinetic product, **M1**, that is 14−16 kcal/mol less stable depending on the solvent (Scheme 3). In addition, the dissociation requires geometric strain and is calculated to involve a barrier of 25−27 kcal/mol. Although this barrier is higher than barriers obtained for the initiation of phosphine-stabilized Ru indenylidene catalysts,[52,53] it is qualitatively consistent with pyridine dissociation taking place at a time scale of hours instead of minutes; see the "Variable-

Scheme 3. Isomerization of Compound 5a

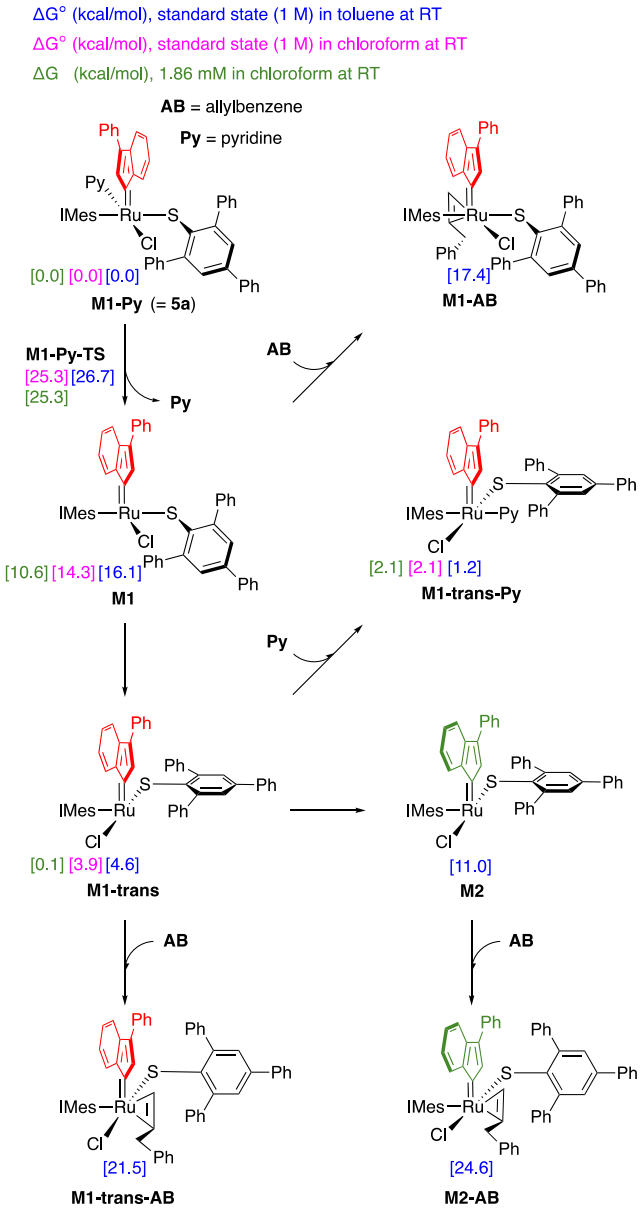

https://dx.doi.org/10.1021/acs.organomet.9b00641
Organometallics XXXX, XXX, XXX−XXX

Temperature ^{1}H NMR Experiments on **5a**" section in the Supporting Information for details. This is much slower than for the closely related alkylidene-based catalysts.[33]

The 14-electron complex, **M1**, generated by pyridine dissociation, may coordinate the olefin to form a π-complex (**M1-AB**) only about 1 kcal/mol less stable than **M1**. However, this π-complex does not have a configuration suitable for cycloaddition and metathesis. Instead of the substrate RHC═CH_2 plane being positioned parallel to that of Ru═Ind, which is required for formation of the new C═C bond, the olefin approaches the indenylidene sideways.

However, metathesis-potent π-complexes may be formed by first isomerizing **M1**. By moving the thiolate from a *cis* to a *trans* position relative to the chloride ligand, **M1-trans** is obtained. The latter complex has, just like the closely related *Z*-selective ruthenium alkylidene catalysts,[33] an empty coordination site *trans* to the NHC ligand and is only 4−5 kcal/mol less stable than **M1-Py**.

Moreover, a transition state for the rearrangement from **M1** to **M1-trans** could not be obtained, but this isomerization is associated with a very soft mode and a negligible barrier. However, even if the rearrangement is fast and the calculated free energy of **M1-trans** is not much higher than that of **M1-Py**, the calculations do not, at first glance, seem to be consistent with the observation (above and in the Supporting Information) that pyridine dissociation from **5a** (= **M1-Py**) is spontaneous. The puzzle is resolved by considering the conditions under which the dissociation experiments were performed: The catalyst was dissolved in $CDCl_3$ at a much lower concentration (1.86 mM) than the standard thermodynamic state (1 M). Correcting for the low concentration of **5a** (as explained in the Supporting Information) leads to the prediction that pyridine dissociation is spontaneous at room temperature (with a relative free energy of **M1-trans** essentially at zero), as observed in the variable-temperature NMR experiments. Under these conditions, i.e., mimicking the low-concentration, variable-temperature ^{1}H NMR experiments as well as the catalytic experiments (which are also conducted at catalyst concentrations closer to 1.86 mM than to 1 M), recoordination of the dissociated pyridine in *trans*-position to the NHC ligand (to give **M1-trans-Py**, Scheme 3) is predicted to be endergonic by 2 kcal/mol. The surprising stability of **M1-trans** is in part due to intramolecular donor−acceptor interactions between one of the ortho-phenyl substituents of the thiolate ligand and the ruthenium center, as shown in Figure 3. Thus, different from **M1** which lacks such stabilizing interactions, **M1-trans** has an effective electron count higher than 14.

The same stabilizing interactions are found for the corresponding active complex (**SM1-trans**, Scheme 4) of SIMes-coordinated catalyst **5b**. DFT calculations (Scheme 4) predict that this active complex is generated from **5b** at approximately the same rate as **M1-trans** from **5a**. The calculated pyridine dissociation barriers (via **SM1-Py-TS** and **M1-Py-TS**, respectively) for the two catalysts are similar. However, the free energy of the active species generated from **5b** (**SM1-trans**) is ca. 1 kcal/mol lower than for **5a**. The higher catalytic activity of **5b** (c.f., entries 1 and 5, Table 1) may thus, at least in part, be due to a stabilizing effect of the SIMes ligand (both a stronger σ-donor and π acceptor than IMes, see above) on the low-coordinate active species. This stabilization shifts the equilibrium between the precursor and the active species more in favor of the latter.

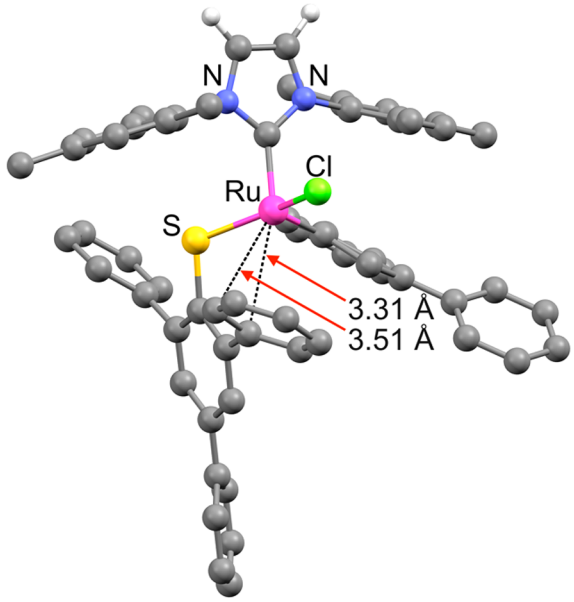

Figure 3. Optimized geometry of **M1-trans** indicating secondary interactions between a thiolate phenyl substituent and ruthenium.

Scheme 4. Isomerization of Compound 5b

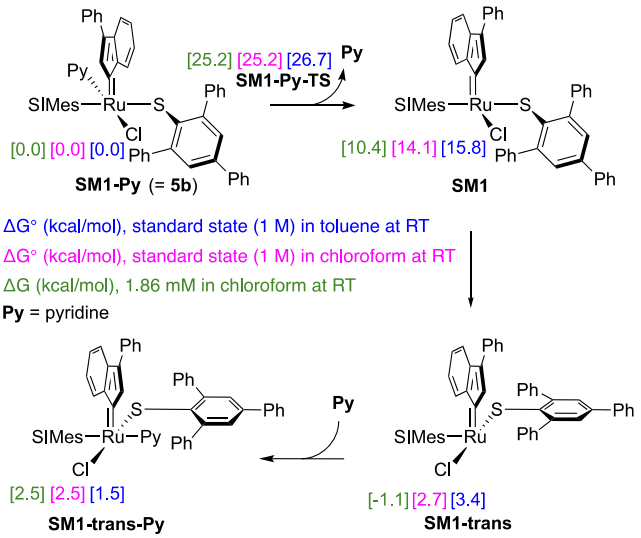

Allylbenzene may bind to the empty coordination site in **M1-trans** to form **M1-trans-AB**, a π-complex that is 4 kcal/mol less stable than **M1-AB**, but which may subsequently evolve via initiation metathesis to replace the indenylidene by a phenylethylidene ready for productive self-metathesis of allylbenzene. That the latter will be *Z*-selective is suggested already by the preferred allylbenzene coordination mode in **M1-trans-AB**, which has the allylbenzene benzyl group oriented away from the bulky thiolate. This allylbenzene orientation is also preferred in the 3 kcal/mol less stable **M2-AB**, which may be formed by a ~180° rotation of indenylidene in **M1-trans** followed by substrate coordination.

We have investigated alternatives to these pyridine dissociation and Ru complex isomerization pathways. First, since the unusual isomer of **5a** and **5b** is due to the steric requirement of the indenylidene, the relatively fast initiation and the *Z*-selectivity of these complexes could, in principle, be due to indenylidene isomerization to the less sterically demanding

https://dx.doi.org/10.1021/acs.organomet.9b00641
Organometallics XXXX, XXX, XXX−XXX

allenylidene.[54−56] However, the allenylidene isomers lie more than 20 kcal/mol higher in energy than the indenylidene counterparts (see the Supporting Information), making them unlikely catalytic intermediates. More importantly, reaching these intermediates is all but impossible, as the indenylidene−allenylidene isomerization barriers have, in general, been found to be prohibitively high.[57] Another possibility is formation of a new catalytic species via secondary bond formation between a thiolate phenyl and ruthenium. Such a bond is formed upon dissociation of chloride from a 14-electron complex. However, even if chloride dissociation from **M2** is compensated for by Ru−phenyl interactions (in **M5**, see the Supporting Information), the energetic cost of reaching **M5** is higher than 30 kcal/mol, effectively excluding chloride dissociation and Ru−phenyl bond formation as part of the initiation mechanism.

In conclusion, while chloride dissociation and indenylidene isomerization to allenylidene are unlikely to take part in the catalyst initiation mechanism, pyridine may dissociate from **M1-Py** (= **5a**) to generate 14-electron complex **M1**. Whereas the latter isomer does not give a metathesis-potent π-complex, it may isomerize to **M1-trans** and **M2**, which both form π-complexes in which the olefin is correctly oriented for cycloaddition. The olefin orientation in these complexes is also indicative of *Z*-selectivity.

The stereodirecting properties of the thiolate ligand have been analyzed using the SambVca web application.[58] The thus-generated steric map of DFT-optimized olefin complex **M1-trans-AB**, with the substrate allylbenzene removed for clarity, is shown in Figure 4. The steric map illustrates, as expected, that

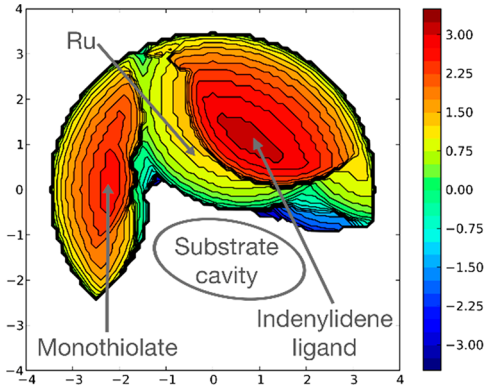

Figure 4. Steric map of **M1-trans-AB** (cf. Scheme 3), obtained for a model in which the atoms of the allylbenzene substrate have been removed.

the thiolate ligand induces *Z*-selectivity by acting on one side of the substrate cavity and forcing substituents to predominantly occupy the other side of the cavity.

To further analyze the steric effects of the thiolate, the percentage of buried volume ($\%V_{Bur}$)[59] of the active species of **5b** (**SM1-trans**, Scheme 4) was compared to that of the corresponding dichloride, i.e., **4** without pyridine, again using DFT-optimized geometries. With 95.0% for **5b** and 86.4% for **4**, respectively, the thiolate is seen to add considerably to the steric congestion. Moreover, only a small part of this difference originates from the sulfur atom itself, i.e., from replacing chlorine with sulfur. When only ruthenium and the atoms directly bonded to ruthenium were considered, $\%V_{Bur}$ was only marginally larger for **5b** (67.7%) than for **4** (67.0%). **5a** experiences a steric congestion very similar to that of **5b**, with a $\%V_{Bur}$ of 67.7% (first coordination sphere) and 94.9% (full model), respectively.

CONCLUSION

The first Ru-monothiolate complexes (**5a** and **5b**) bearing indenylidene ligands have been prepared. These complexes contain three sterically demanding ligands: the NHC, the arylthiolate, and the indenylidene. The resulting steric pressure forces the thiolate ligand to position itself *trans* to the NHC ligand. This ligand configuration is not found in any other monothiolate-based OM catalyst. In fact, this configuration is both incompatible with *Z*-selectivity and expected to initiate metathesis slowly as pyridine might not readily dissociate when *trans* to a chloride. Surprisingly, even though this dissociation is indeed associated with a barrier, **5a** and **5b** not only initiate more rapidly than their 2-isopropoxybenzylidene congeners but also are fairly long-lived (TONs up to 2200) and *Z*-selective, offering up to ca. 80% of the *Z*-isomer in prototypical metathesis homocoupling reactions.

To uncover the causes behind the unexpected selectivity and fairly rapid initiation, the initial pyridine dissociation and the subsequent rearrangement into isomers expected to be *Z*-selective were investigated using DFT. The calculations confirmed a barrier (25−27 kcal/mol) to pyridine dissociation, reflecting the cost of generating an empty coordination site *trans* to chloride in 14-electron complex **M1**. Next, the empty coordination site in **M1** may be taken up by the thiolate to give much more stable **M1-trans**, which may bind allylbenzene to form a π-complex (**M1-trans-AB**). The latter may subsequently evolve via initiation metathesis to mediate productive self-metathesis of allylbenzene. That this metathesis is *Z*-selective is indicated already by the preferred orientation, away from the bulky thiolate, of the allylbenzene benzyl group in **M1-trans-AB**.

EXPERIMENTAL SECTION

Unless otherwise stated, reactions were performed under a dry argon atmosphere by using Schlenk techniques or a glovebox. [$RuCl_2$(IMes)-$(Py)_2$(3-phenylindenylidene)] (**3b**) and potassium 2,4,6-triphenylbenzene-thiolate were prepared according to their respective literature procedures.[27,30] [$RuCl_2$(SIMes)(Py)(3-phenylindenylidene)] (**4**), commercially available as Umicore M31, was obtained from Sigma-Aldrich and used as received. Inhibitor-free THF, obtained from Sigma-Aldrich, was dried over potassium hydride and filtered over Celite prior to use. Anhydrous *n*-pentane was purchased from Sigma-Aldrich and used as received. DCM was dried using an MBraun solvent purification system ("Grubbs column") before use. Allylbenzene, 1-octene, 4-phenyl-1-butene, and pyridine were obtained from Sigma-Aldrich. Allylbenzene and 4-phenyl-1-butene were degassed, dried overnight over CaH_2, filtered over a pad of activated basic alumina (Brockmann I), and stored overnight over activated Selexsorb CD. 1-Octene was degassed and filtered over a pad of activated basic alumina (Brockmann I).

NMR spectra were recorded on Bruker Biospin AV500, AV600, and 850 Ascend spectrometers. Chemical shifts were reported relative to the residual solvent peaks.[60] HRMS ESI mass spectra were recorded by means of an orthogonal electron spray ionization ion source (ESI) interfaced to a JMS-T100LC AccuTOF mass spectrometer from JEOL USA, Inc. (Peabody, MA). The ions were transported into the orthogonal accelerating time-of-flight (TOF) single-stage reflectron mass analyzer by a high-frequency and high-voltage quadrupole ion guide. Detection was achieved with a dual microchannel plate detector. Elemental analyses were performed using an Elementar Vario EL III analyzer.

Suitable crystals for diffraction experiments were immersed in Paratone-N (Hampton Research) in a nylon loop. Data collection was done on a Bruker AXS TXS rotating anode system with an APEXII Pt[135]

https://dx.doi.org/10.1021/acs.organomet.9b00641
Organometallics XXXX, XXX, XXX−XXX

CCD detector using graphite-monochromated Mo Kα radiation (λ = 0.71073 Å). Data collection and data processing were done using APEX2,[61] SAINT,[62] and SADABS[63] version 2008/1 or TWINABS,[64] whereas structure solution and final model refinement were done using SHELXS[65] version 2013/1 or SHELXT[66] version 2014/4 and SHELXL[67] version 2014/7.

[RuCl(IMes)(-*S*-2,4,6-Ph-C_6H_2)(Py)(3-phenylindenylidene)] (5a). Under an inert atmosphere, [$RuCl_2$(IMes)$(Py)_2$(3-phenylindenylidene)] (**3b**, 100.0 mg, 0.121 mmol) and potassium 2,4,6-triphenylbenzenethiolate (47.6 mg, 0.126 mmol) were suspended in 5 mL of THF. After 2 h of stirring at room temperature, the mixture was filtered through a short pad of Celite. Subsequently, the filtrate was concentrated to about 2 mL *in vacuo*. Slow addition of 3 mL of *n*-pentane yielded after 1 day at −32 °C dark-red microcrystals (92 mg, yield 72%) of **5a**. Crystals suitable for X-ray diffraction analysis were grown by slow diffusion of pentane into a concentrate solution of **5a** in dichloromethane at −32 °C. ^{1}H NMR (850.13 MHz, $CDCl_3$): δ = 8.62 (br m, 0.401H), 8.49 (d, $^3J_{HH}$ = 5.5 Hz, 0.77H), 8.13 (br d, $^3J_{HH}$ = 7.1 Hz, 1.57H), 7.90 (d, $^4J_{HH}$ = 2.0 Hz 0.19H), 7.72−7.27 (m, 14.38H), 7.23−7.18 (m, 2,13H), 7.11 (d, $^3J_{HH}$ = 2.0 Hz, 0.19H), 7.08−6.99 (m, 3.53H), 6.95 (td, $^3J_{HH}$ = 7.1 and $^4J_{HH}$ = 1.0 Hz, 0.79H), 6.87−6.77 (m, 3.55H), 6.58−651 (m, 0.51H), 6.44−6.39 (m, 1.60H), 6.29 (nr m, 1.70H), 6.17 (s, 1.58H), 6.00−5.93 (m, 2.70H), 5.86 (t, $^3J_{HH}$ = 5.9 Hz, 0.20H), 5.77 (d, $^3J_{HH}$ = 7.8 Hz, 0.20H), 5.25 (br d, $^3J_{HH}$ = 5.7 Hz, 0.20H), 5.22 (br d, $^3J_{HH}$ = 7.3 Hz, 0.79H), 5.19 (br t, $^3J_{HH}$ = 5.7 Hz, 0.20H), 5.11 (s, 0.19H), 4.17 (t, $^3J_{HH}$ = 6.2 Hz, 0.20H), 2.38 (s, 2.33H), 2.34 (s, 0.62H), 2.31 (s, 2.33H), 2.26 (s, 0.62H), 2.21 (s, 2.32H), 2.16 (s, 0.62H), 2.10 (s, 0.61H), 2.07 (s, 0.62H), 1.65 (s, 2.31H), 1.64 (s, 0.63H), 1.58 (s, 2.31H), 1.02 (s, 2.33H). ^{13}C{^{1}H} NMR (150.91 MHz, $CDCl_3$): δ = 270.76, 183.30, 180.29, 159.11, 154.02, 150.02, 149.75, 147.97, 147.61, 146.70, 145.50, 145.14, 142.85, 142.81, 142.69, 141.53, 141.13, 140.49, 140.09, 139.64, 139.58, 139.14, 139.04, 138.76, 138.58, 138.03, 137.33, 137.25, 137.09, 137.04, 136.79, 136.67, 135.99, 135.95, 135.90, 135.46, 134.61, 134.54, 134.09, 133.76, 133.69, 132.97, 131.96, 130.74, 130.34, 130.00, 129.87, 129.73, 129.50, 129.43, 129.26, 129.21, 129.14, 129.09, 128.67, 128.43, 128.36, 128.22, 128.06, 127.86, 127.72, 127.64, 127.64, 127.45, 127.27, 127.14, 126.91, 126.82, 126.68, 126.55, 126.46, 126.35, 126.27, 125.88, 125.77, 125.58, 125.35, 125.31, 125.11, 124.38, 124.33, 123.98, 123.84, 123.40, 122.48, 121.56, 117.38, 99.73, 93.89, 90.89, 89.46, 87.79, 78.93, 63.75, 21.20, 21.13, 20.96, 20.90, 20.79, 20.15, 20.01, 19.84, 19.57, 18.59, 18.42, 18.23. Anal. Calcd (%) for $C_{65}H_{56}ClN_3RuS$: C 74.51, H 5.39, N 4.01. Found: C 74.42, H 5.34, N 4.00. HRMS (ESI$^+$) found (calcd): *m*/*z* 933.28172 (933.28164) [$C_{60}H_{51}N_2{}^{102}RuS$]$^+$.

[RuCl(SIMes)(-*S*-2,4,6-Ph-C_6H_2)(Py)(3-phenylindenylidene)] (5b). Under an inert atmosphere, [$RuCl_2$(SIMes)(Py)(3-phenylindenylidene)] (**4**, 99.7 mg, 0.133 mmol) and potassium 2,4,6-triphenylbenzenethiolate (52.3 mg, 0.139 mmol) where suspended in 5 mL of THF. After 30 min of stirring at room temperature, the mixture was filtered over a glass fiber filter. The residue on the filter was dissolved in DCM. Subsequent addition of *n*-pentane yielded a precipitate. The precipitate was first washed with a small amount of *n*-pentane, then dried and finally redissolved in DCM. Slow addition of 3 mL of *n*-pentane yielded after some days at −32 °C dark-red microcrystals (28.4 mg, yield 20%) of **5b**. ^{1}H NMR (850.13 MHz, $CDCl_3$): δ = 8.61 (br, 1.34H), 8.28 (br, 0.37H), 8.12 (br d, $^3J_{HH}$ = 6.7 Hz, 0.73H), 7.86 (d, $^3J_{HH}$ = 1.8 Hz, 0.62H), 7.75 (br d, $^3J_{HH}$ = 7.7 Hz, 0.64H), 7.71−7.66 (m, 1.88 H), 7.64−7.58 (m, 1.65H), 7.56−7.26 (m, 10.23H), 7.23 (br t, $^3J_{HH}$ = 7.7 Hz, 0.78H), 7.19 (br t, $^3J_{HH}$ = 7.3 Hz, 0.34H), 7.06 (br s, 0.57H), 7.04 (br s, 0.31H), 7.02−6.99 (m, 0.96H), 6.98 (br s, 0.68H), 6.92 (t d, $^3J_{HH}$ = 7.2, 0.7 Hz, 0.33H), 6.87 (br t, $^3J_{HH}$ = 5.6 Hz, 0.32H), 6.82−6.75 (m, 1.48H), 6.54 (br, 1.11H), 6.50 (br t, $^3J_{HH}$ = 6.1 Hz, 0.37H), 6.41 (t d, $^3J_{HH}$ = 7.1, 0.7 Hz, 0.37H), 6.36 (d, $^3J_{HH}$ = 6.0 Hz, 0.64H), 6.27 (br, 0.77H), 6.24 (br s, 0.66H), 6.19 (br s, 0.38H), 6.06 (s, 0.62H), 6.00 (d, $^3J_{HH}$ = 7.0 Hz, 0.74H), 5.94 (br t, $^3J_{HH}$ = 6.9 Hz, 0.37H), 5.91 (t, $^3J_{HH}$ = 6.0 Hz, 0.64H), 5.85 (s, 0.37H), 5.74 (d, $^3J_{HH}$ = 8.1 Hz, 0.73H), 5.24 (d, $^3J_{HH}$ = 7.4 Hz, 0.37H), 5.21 (d, $^3J_{HH}$ = 5.4 Hz, 0.64H), 5.10 (t, $^3J_{HH}$ = 5.8 Hz, 0.64H), 4.11 (t, $^3J_{HH}$ = 6.1 Hz, 0.63H), 4.04−3.90 (m, 1.82H), 3.89−3.79 (m, 0.62H), 3.79−3.70 (m, 0.74H), 3.65−3.53 (m, 0.96H), 2.65 (s, 1.09H), 2.52 (m, 3.76H), 2.44 (s, 1.11H), 2.29 (s, 1.80H), 2.26 (s, 1.88H), 2.15 (s, 1,90H), 2.10 (s, 1.82H), 1.73 (s, 1.11H), 1.67 (s, 1.84H), 1.57 (s, 1.11H), 1.16 (s, 1.11H). ^{13}C{^{1}H} NMR (213.77 MHz, $CDCl_3$): δ = 271.16, 215.07, 211.21, 159.17, 156.85, 154.61, 151.77, 149.93, 147.98, 147.72, 146.60, 145.50, 145.14, 143.00, 142.91, 142.60, 142.52, 141.71, 141.57, 141.39, 141.19, 140.36, 140.07, 139.91, 139.75, 139.55, 139.07, 138.79, 128.67, 138.19, 138.07, 137.97, 137.87, 137.63, 137.59, 137.56, 137.36, 137.14, 137.02, 136.86, 136.76, 136.53, 136.30, 136.02, 135.78, 135.01, 134.83, 134.61, 134.44, 133.85, 131.97, 130.99, 130.65, 130.13, 130.08, 130.04, 129.94, 129.79, 129.68, 129.54, 129.44, 129.26, 129.21, 129.09, 129.02, 128.98, 128.88, 128.86, 128.81, 128.77, 128.47, 128.37, 128.23, 128.14, 128.11, 128.07, 128.04, 127.98, 127.95, 127.84, 127.74, 127.66, 127.60, 127.53 127.50, 127.30, 127.18, 127.03, 127.01, 126.96, 126.91, 127.71, 126.67, 126.57, 126.47, 126.40, 126.36, 125.99, 125.72, 125.31, 124.61, 124.31, 124.05, 123.19, 122.47, 121.56, 121.29, 117.44, 116.62, 100.37, 99.95, 94.67, 91.81, 89.88, 87.41, 79.40, 62.50, 54.35, 53.68, 53.56, 53.11, 52.67, 51.31, 50.88, 34.27, 31.74, 22.49, 21.21, 21.12, 21.05, 20.98, 20.96, 20.90, 20.80, 20.23, 20.04, 19.82, 19.47, 19.15, 18.83, 18.45, 18.25, 17.82, 14.21. Anal. Calcd (%) for $C_{65}H_{58}ClN_3RuS$: C 74.37, H 5.57, N 4.00. Found: C 74.35, H 5.29, N 3.96. HRMS (ESI$^+$) found (calcd): *m*/*z* 1072.3026 (1072.2981) [$C_{65}H_{58}{}^{35}ClN_3{}^{102}RuS$ +Na]$^+$.

Catalytic Tests, General Procedure. In a glovebox, a 4 mL vial equipped with a magnetic stirring bar and a screw cap was charged with the substrate, 2 mg of hexamethylbenzene (internal standard), and the catalyst. The vial was closed, and the reaction mixture was stirred at room temperature. The reaction was quenched with an excess of ethyl vinyl ether (EVE). Determination of conversions, O/I ratio, and *Z*-selectivities were done according to literature procedures.[29,36]

For catalyst loading of 0.5 mol %, 0.50 mmol of substrate and 0.0025 mmol of catalyst were used.

For catalyst loading of 0.1 mol %, 0.76 mmol of substrate and 0.00076 mmol of catalyst were used.

For catalyst loading of 0.01 mol %, 7.6 mmol of substrate and 0.00076 mmol of catalyst were used.

In the catalytic tests with pyridine, the small amount of pyridine (0.02 mg) was added by preparing a stock solution of pyridine in the substrate. The stock solution was obtained by dilution of another stock solution prepared by dissolving 1 mg of pyridine into 2.5 mmol of substrate [e.g., 10-fold dilution (0.1 equiv), 5-fold dilution (0.2 equiv), no dilution (1.0 equiv), and 50-fold dilution (Table 1, entry 4)].

■ ASSOCIATED CONTENT

Supporting Information

The Supporting Information is available free of charge at https://pubs.acs.org/doi/10.1021/acs.organomet.9b00641.

Spectra (^{1}H, ^{13}C NMR, and HRMS) and X-ray refinement data for new compounds, computational details, calculated electronic and free energies, and additional computational results (PDF)

Computed molecular Cartesian coordinates in a format convenient for visualization (XYZ)

Accession Codes

CCDC 1942925 and 1942926 contain the supplementary crystallographic data for this paper. These data can be obtained free of charge via www.ccdc.cam.ac.uk/data_request/cif, or by emailing data_request@ccdc.cam.ac.uk, or by contacting The Cambridge Crystallographic Data Centre, 12 Union Road, Cambridge CB2 1EZ, UK; fax: +44 1223 336033.

■ AUTHOR INFORMATION

Corresponding Authors

Giovanni Occhipinti − *Department of Chemistry, University of Bergen N-5007 Bergen, Norway;* orcid.org/0000-0002-7279-6322; Email: Giovanni.Occhipinti@uib.no

https://dx.doi.org/10.1021/acs.organomet.9b00641
Organometallics XXXX, XXX, XXX−XXX

Vidar R. Jensen − *Department of Chemistry, University of Bergen N-5007 Bergen, Norway;* orcid.org/0000-0003-2444-3220; Email: Vidar.Jensen@uib.no

Authors

Wietse Smit − *Department of Chemistry, University of Bergen N-5007 Bergen, Norway;* orcid.org/0000-0002-0142-6025

Jonas B. Ekeli − *Department of Chemistry, University of Bergen N-5007 Bergen, Norway;* orcid.org/0000-0002-6137-6322

Bartosz Woźniak − *Department of Chemistry, University of Bergen N-5007 Bergen, Norway;* orcid.org/0000-0002-7460-3344

Karl W. Törnroos − *Department of Chemistry, University of Bergen N-5007 Bergen, Norway;* orcid.org/0000-0001-6140-5915

Complete contact information is available at: https://pubs.acs.org/10.1021/acs.organomet.9b00641

Notes

The authors declare no competing financial interest.

■ ACKNOWLEDGMENTS

We gratefully acknowledge financial support from the Research Council of Norway (RCN) via the GASSMAKS (grant no. 208335), FORNY2020 (239288), and FRIPRO (262370) programs, as well as via the Norwegian NMR Platform, NNP (226244). The RCN is also thanked for CPU (NN2506K) and storage resources (NS2506K). Bjarte Holmelid is thanked for assistance with the HRMS ESI$^+$) analyses and Inger Johanne Fjellanger for assistance with the elemental analysis. W.S. is grateful to the University of Bergen for a Ph.D. scholarship.

■ REFERENCES

(1) Bazan, G. C.; Khosravi, E.; Schrock, R. R.; Feast, W. J.; Gibson, V. C.; O'Regan, M. B.; Thomas, J. K.; Davis, W. M. Living Ring-Opening Metathesis Polymerization of 2,3-Difunctionalized Norbornadienes by Mo(:CHBu-tert)(:NC_6H_3Pr-iso$_2$-2,6)(OBu-tert)$_2$. *J. Am. Chem. Soc.* **1990**, *112*, 8378−8387.

(2) Bazan, G. C.; Oskam, J. H.; Cho, H. N.; Park, L. Y.; Schrock, R. R. Living Ring-Opening Metathesis Polymerization of 2,3-Difunctionalized 7-Oxanorbornenes and 7-Oxanorbornadienes by Mo(CHCMe$_2$R)(NC_6H_3-iso-Pr$_2$-2,6)(O-tert-Bu)$_2$ and Mo(CHCMe$_2$R)(NC_6H_3-iso-Pr$_2$-2,6)($OCMe_2CF_3$)$_2$. *J. Am. Chem. Soc.* **1991**, *113*, 6899−6907.

(3) Nguyen, S. T.; Grubbs, R. H.; Ziller, J. W. Syntheses and Activities of New Single-Component, Ruthenium-Based Olefin Metathesis Catalysts. *J. Am. Chem. Soc.* **1993**, *115*, 9858−9859.

(4) Nguyen, S. T.; Johnson, L. K.; Grubbs, R. H.; Ziller, J. W. Ring-Opening Metathesis Polymerization (ROMP) of Norbornene by a Group VIII Carbene Complex in Protic Media. *J. Am. Chem. Soc.* **1992**, *114*, 3974−3975.

(5) Schrock, R. R.; DePue, R. T.; Feldman, J.; Schaverien, C. J.; Dewan, J. C.; Liu, A. H. Preparation and Reactivity of Several Alkylidene Complexes of the Type W(CHR')(N-2,6-C_6H_3-iso-Pr$_2$)(OR)$_2$ and Related Tungstacyclobutane Complexes. Controlling Metathesis Activity through the Choice of Alkoxide Ligand. *J. Am. Chem. Soc.* **1988**, *110*, 1423−1435.

(6) Schrock, R. R.; Murdzek, J. S.; Bazan, G. C.; Robbins, J.; DiMare, M.; O'Regan, M. Synthesis of Molybdenum Imido Alkylidene Complexes and Some Reactions Involving Acyclic Olefins. *J. Am. Chem. Soc.* **1990**, *112*, 3875−3886.

(7) Schwab, P.; France, M. B.; Ziller, J. W.; Grubbs, R. H. A Series of Well-Defined Metathesis Catalysts−Synthesis of [$RuCl_2$(=CHR')(PR_3)$_2$] and Its Reactions. *Angew. Chem., Int. Ed. Engl.* **1995**, *34*, 2039−2041.

(8) Schwab, P.; Grubbs, R. H.; Ziller, J. W. Synthesis and Applications of $RuCl_2$(CHR')(PR_3)$_2$: The Influence of the Alkylidene Moiety on Metathesis Activity. *J. Am. Chem. Soc.* **1996**, *118*, 100−110.

(9) Scholl, M.; Ding, S.; Lee, C. W.; Grubbs, R. H. Synthesis and Activity of a New Generation of Ruthenium-Based Olefin Metathesis Catalysts Coordinated with 1,3-Dimesityl-4,5-dihydroimidazol-2-ylidene Ligands. *Org. Lett.* **1999**, *1*, 953−956.

(10) Dragutan, V.; Dragutan, I.; Verpoort, F. Ruthenium Indenylidene Complexes. *Platinum Met. Rev.* **2005**, *49*, 33−40.

(11) Jafarpour, L.; Schanz, H.-J.; Stevens, E. D.; Nolan, S. P. Indenylidene-Imidazolylidene Complexes of Ruthenium as Ring-Closing Metathesis Catalysts. *Organometallics* **1999**, *18*, 5416−5419.

(12) Harlow, K. J.; Hill, A. F.; Wilton-Ely, J. D. E. T. The First Co-Ordinatively Unsaturated Group 8 Allenylidene Complexes: Insights into Grubbs' *vs.* Dixneuf-Fürstner Olefin Metathesis Catalysts. *J. Chem. Soc., Dalton Trans.* **1999**, 285−292.

(13) Fürstner, A.; Guth, O.; Düffels, A.; Seidel, G.; Liebl, M.; Gabor, B.; Mynott, R. Indenylidene Complexes of Ruthenium: Optimized Synthesis, Structure Elucidation, and Performance as Catalysts for Olefin Metathesis—Application to the Synthesis of the ADE-Ring System of Nakadomarin A. *Chem. - Eur. J.* **2001**, *7*, 4811−4820.

(14) Furstner, A.; Liebl, M.; Hill, A. F.; Wilton-Ely, J. D. E. T. Coordinatively Unsaturated Ruthenium Allenylidene Complexes: Highly Effective, Well Defined Catalysts for the Ring-Closure Metathesis of α,ω-Dienes and Dienynes. *Chem. Commun.* **1999**, 601−602.

(15) Fürstner, A.; Grabowski, J.; Lehmann, C. W. Total Synthesis and Structural Refinement of the Cyclic Tripyrrole Pigment Nonylprodigiosin. *J. Org. Chem.* **1999**, *64*, 8275−8280.

(16) Boeda, F.; Clavier, H.; Nolan, S. P. Ruthenium-Indenylidene Complexes: Powerful Tools for Metathesis Transformations. *Chem. Commun.* **2008**, 2726−2740.

(17) Fürstner, A.; Thiel, O. R.; Ackermann, L.; Schanz, H.-J.; Nolan, S. P. Ruthenium Carbene Complexes with N, N′-Bis(Mesityl)Imidazol-2-Ylidene Ligands: RCM Catalysts of Extended Scope. *J. Org. Chem.* **2000**, *65*, 2204−2207.

(18) Schmidt, B.; Wildemann, H. Single and Double Ring Closing Metathesis in the Formation of Dihydropyrans and Bisoxacyclic Systems with a Quaternary Centre. *J. Chem. Soc., Perkin Trans.* **2000**, *1*, 2916−2925.

(19) Fürstner, A.; Thiel, O. R. Formal Total Synthesis of (−)-Balanol: Concise Approach to the Hexahydroazepine Segment Based on RCM. *J. Org. Chem.* **2000**, *65*, 1738−1742.

(20) Fürstner, A.; Grabowski, J.; Lehmann, C. W.; Kataoka, T.; Nagai, K. Synthesis and Biological Evaluation of Nonylprodigiosin and Macrocyclic Prodigiosin Analogues. *ChemBioChem* **2001**, *2*, 60−68.

(21) Fürstner, A.; Jeanjean, F.; Razon, P. Total Synthesis of Woodrosin I. *Angew. Chem., Int. Ed.* **2002**, *41*, 2097−2101.

(22) Scheiper, B.; Glorius, F.; Leitner, A.; Fürstner, A. Catalysis-Based Enantioselective Total Synthesis of the Macrocyclic Spermidine Alkaloid Isooncinotine. *Proc. Natl. Acad. Sci. U. S. A.* **2004**, *101*, 11960−11965.

(23) Fürstner, A.; Radkowski, K.; Wirtz, C.; Goddard, R.; Lehmann, C. W.; Mynott, R. Total Syntheses of the Phytotoxic Lactones Herbarumin I and II and a Synthesis-Based Solution of the Pinolidoxin Puzzle. *J. Am. Chem. Soc.* **2002**, *124*, 7061−7069.

(24) Lecourt, C.; Boinapally, S.; Dhambri, S.; Boissonnat, G.; Meyer, C.; Cossy, J.; Sautel, F.; Massiot, G.; Ardisson, J.; Sorin, G.; Lannou, M.-I. Elaboration of Sterically Hindered Δ-Lactones through Ring-Closing Metathesis: Application to the Synthesis of the C1−C27 Fragment of Hemicalide. *J. Org. Chem.* **2016**, *81*, 12275−12290.

(25) Love, J. A.; Morgan, J. P.; Trnka, T. M.; Grubbs, R. H. A Practical and Highly Active Ruthenium-Based Catalyst That Effects the Cross Metathesis of Acrylonitrile. *Angew. Chem., Int. Ed.* **2002**, *41*, 4035−4037.

(26) Clavier, H.; Petersen, J. L.; Nolan, S. P. A Pyridine-Containing Ruthenium−Indenylidene Complex: Synthesis and Activity in Ring-Closing Metathesis. *J. Organomet. Chem.* **2006**, *691*, 5444−5447.

(27) Clavier, H.; Nolan, S. P.; İmamoğlu, Y.; Dragutan, V. Synthesis and Activity in Ring-Closing Metathesis of Phosphine and NHC-Containing Ruthenium−Indenylidene (Bis)Pyridine Complexes. In *Metathesis Chemistry. NATO Sci. Ser., II* İmamoğlu, Y., Dragutan, V., Karabulut, S., Eds.; Springer: Dordrecht, The Netherlands, 2007; Vol. *243*, pp 29−37.
(28) Burtscher, D.; Lexer, C.; Mereiter, K.; Winde, R.; Karch, R.; Slugovc, C. Controlled Living Ring-Opening Metathesis Polymerization with a Ruthenium Indenylidene Initiator. *J. Polym. Sci., Part A: Polym. Chem.* **2008**, *46*, 4630−4635.
(29) Occhipinti, G.; Hansen, F. R.; Törnroos, K. W.; Jensen, V. R. Simple and Highly *Z*-Selective Ruthenium-Based Olefin Metathesis Catalyst. *J. Am. Chem. Soc.* **2013**, *135*, 3331−3334.
(30) Occhipinti, G.; Koudriavtsev, V.; Törnroos, K. W.; Jensen, V. R. Theory-Assisted Development of a Robust and *Z*-Selective Olefin Metathesis Catalyst. *Dalton Trans.* **2014**, *43*, 11106−11117.
(31) Smit, W.; Koudriavtsev, V.; Occhipinti, G.; Törnroos, K. W.; Jensen, V. R. Phosphine-Based *Z*-Selective Ruthenium Olefin Metathesis Catalysts. *Organometallics* **2016**, *35*, 1825−1837.
(32) Renom-Carrasco, M.; Mania, P.; Sayah, R.; Veyre, L.; Occhipinti, G.; Gajan, D.; Lesage, A.; Jensen, V. R.; Thieuleux, C. Supported Ru Olefin Metathesis Catalysts *via* a Thiolate Tether. *Dalton Trans.* **2019**, *48*, 2886−2890.
(33) Occhipinti, G.; Törnroos, K. W.; Jensen, V. R. Pyridine-Stabilized Fast-Initiating Ruthenium Monothiolate Catalysts for *Z*-Selective Olefin Metathesis. *Organometallics* **2017**, *36*, 3284−3292.
(34) Jensen, V. R.; Occhipinti, G. Improved Olefin Metathesis Catalysts. U.S. Patent 10265691 B2, 2019.
(35) Endo, K.; Grubbs, R. H. Chelated Ruthenium Catalysts for *Z*-Selective Olefin Metathesis. *J. Am. Chem. Soc.* **2011**, *133*, 8525−8527.
(36) Keitz, B. K.; Endo, K.; Herbert, M. B.; Grubbs, R. H. *Z*-Selective Homodimerization of Terminal Olefins with a Ruthenium Metathesis Catalyst. *J. Am. Chem. Soc.* **2011**, *133*, 9686−9688.
(37) Keitz, B. K.; Endo, K.; Patel, P. R.; Herbert, M. B.; Grubbs, R. H. Improved Ruthenium Catalysts for *Z*-Selective Olefin Metathesis. *J. Am. Chem. Soc.* **2012**, *134*, 693−699.
(38) Rosebrugh, L. E.; Herbert, M. B.; Marx, V. M.; Keitz, B. K.; Grubbs, R. H. Highly Active Ruthenium Metathesis Catalysts Exhibiting Unprecedented Activity and *Z*-Selectivity. *J. Am. Chem. Soc.* **2013**, *135*, 1276−1279.
(39) Khan, R. K. M.; Torker, S.; Hoveyda, A. H. Readily Accessible and Easily Modifiable Ru-Based Catalysts for Efficient and *Z*-Selective Ring-Opening Metathesis Polymerization and Ring-Opening/Cross-Metathesis. *J. Am. Chem. Soc.* **2013**, *135*, 10258−10261.
(40) Koh, M. J.; Khan, R. K. M.; Torker, S.; Hoveyda, A. H. Broadly Applicable *Z*- and Diastereoselective Ring-Opening/Cross-Metathesis Catalyzed by a Dithiolate Ru Complex. *Angew. Chem., Int. Ed.* **2014**, *53*, 1968−1972.
(41) Koh, M. J.; Khan, R. K. M.; Torker, S.; Yu, M.; Mikus, M. S.; Hoveyda, A. H. High-Value Alcohols and Higher-Oxidation-State Compounds by Catalytic *Z*-Selective Cross-Metathesis. *Nature* **2015**, *517*, 181−186.
(42) Jensen, V. R.; Occhipinti, G.; Hansen, F. R. Novel Olefin Metathesis Catalysts. WO2012032131A1, 2012.
(43) Pump, E.; Cavallo, L.; Slugovc, C. A Theoretical View on the Thermodynamic *cis*−*trans* Equilibrium of Dihalo Ruthenium Olefin Metathesis (Pre-)Catalysts. *Monatsh. Chem.* **2015**, *146*, 1131−1141.
(44) Occhipinti, G.; Bjørsvik, H.-R.; Jensen, V. R. Quantitative Structure-Activity Relationships of Ruthenium Catalysts for Olefin Metathesis. *J. Am. Chem. Soc.* **2006**, *128*, 6952−6964.
(45) Clavier, H.; Nolan, S. P. N-Heterocyclic Carbene and Phosphine Ruthenium Indenylidene Precatalysts: A Comparative Study in Olefin Metathesis. *Chem. - Eur. J.* **2007**, *13*, 8029−8036.
(46) Rouen, M.; Borré, E.; Falivene, L.; Toupet, L.; Berthod, M.; Cavallo, L.; Olivier-Bourbigou, H.; Mauduit, M. Cycloalkyl-Based Unsymmetrical Unsaturated (U2)-NHC Ligands: Flexibility and Dissymmetry in Ruthenium-Catalysed Olefin Metathesis. *Dalton Trans.* **2014**, *43*, 7044−7049.
(47) Voccia, M.; Nolan, S. P.; Cavallo, L.; Poater, A. The Activity of Indenylidene Derivatives in Olefin Metathesis Catalysts. *Beilstein J. Org. Chem.* **2018**, *14*, 2956−2963.
(48) Muñoz, S. B.; Fleischauer, V. E.; Brennessel, W. W.; Neidig, M. L. Combined Effects of Backbone and N-Substituents on Structure, Bonding, and Reactivity of Alkylated Iron(II)-NHCs. *Organometallics* **2018**, *37*, 3093−3101.
(49) Benitez, D.; Goddard, W. A. The Isomerization Equilibrium between Cis and Trans Chloride Ruthenium Olefin Metathesis Catalysts from Quantum Mechanics Calculations. *J. Am. Chem. Soc.* **2005**, *127*, 12218−12219.
(50) Jensen, V. R.; Occhipinti, G. Ruthenium and Osmium Heterocyclic Carbene Metathesis Catalysts. U.S. Patent 9,303,100 B2, 2016.
(51) Engel, J.; Smit, W.; Foscato, M.; Occhipinti, G.; Törnroos, K. W.; Jensen, V. R. Loss and Reformation of Ruthenium Alkylidene: Connecting Olefin Metathesis, Catalyst Deactivation, Regeneration, and Isomerization. *J. Am. Chem. Soc.* **2017**, *139*, 16609−16619.
(52) Urbina-Blanco, C. A.; Poater, A.; Lebl, T.; Manzini, S.; Slawin, A. M. Z.; Cavallo, L.; Nolan, S. P. The Activation Mechanism of Ru−Indenylidene Complexes in Olefin Metathesis. *J. Am. Chem. Soc.* **2013**, *135*, 7073−7079.
(53) Manzini, S.; Urbina Blanco, C. A.; Nelson, D. J.; Poater, A.; Lebl, T.; Meiries, S.; Slawin, A. M. Z.; Falivene, L.; Cavallo, L.; Nolan, S. P. Evaluation of an Olefin Metathesis Pre-Catalyst with a Bulky and Electron-Rich N-Heterocyclic Carbene. *J. Organomet. Chem.* **2015**, *780*, 43−48.
(54) Fürstner, A.; Picquet, M.; Bruneau, C.; Dixneuf, P. H. Cationic Ruthenium Allenylidene Complexes as a New Class of Performing Catalysts for Ring Closing Metathesis. *Chem. Commun.* **1998**, 1315−1316.
(55) Castarlenas, R.; Dixneuf, P. H. Highly Active Catalysts in Alkene Metathesis: First Observed Transformation of Allenylidene into Indenylidene Via Alkenylcarbyne—Ruthenium Species. *Angew. Chem., Int. Ed.* **2003**, *42*, 4524−4527.
(56) Castarlenas, R.; Vovard, C.; Fischmeister, C.; Dixneuf, P. H. Allenylidene-to-Indenylidene Rearrangement in Arene-Ruthenium Complexes: A Key Step to Highly Active Catalysts for Olefin Metathesis Reactions. *J. Am. Chem. Soc.* **2006**, *128*, 4079−4089.
(57) Pump, E.; Slugovc, C.; Cavallo, L.; Poater, A. Mechanism of the Ru-Allenylidene to Ru-Indenylidene Rearrangement in Ruthenium Precatalysts for Olefin Metathesis. *Organometallics* **2015**, *34*, 3107−3111.
(58) Falivene, L.; Cao, Z.; Petta, A.; Serra, L.; Poater, A.; Oliva, R.; Scarano, V.; Cavallo, L. Towards the Online Computer-Aided Design of Catalytic Pockets. *Nat. Chem.* **2019**, *11*, 872−879.
(59) Hillier, A. C.; Sommer, W. J.; Yong, B. S.; Petersen, J. L.; Cavallo, L.; Nolan, S. P. A Combined Experimental and Theoretical Study Examining the Binding of N-Heterocyclic Carbenes (NHC) to the Cp*RuCl (Cp* = η^5-C_5Me_5) Moiety: Insight into Stereoelectronic Differences between Unsaturated and Saturated NHC Ligands. *Organometallics* **2003**, *22*, 4322−4326.
(60) Fulmer, G. R.; Miller, A. J. M.; Sherden, N. H.; Gottlieb, H. E.; Nudelman, A.; Stoltz, B. M.; Bercaw, J. E.; Goldberg, K. I. NMR Chemical Shifts of Trace Impurities: Common Laboratory Solvents, Organics, and Gases in Deuterated Solvents Relevant to the Organometallic Chemist. *Organometallics* **2010**, *29*, 2176−2179.
(61) *Apex2*, version 2014.11−0; Bruker-AXS: Madison, WI, 2014.
(62) *Saint*, version 7.68A; Bruker-AXS: Madison, WI, 2010.
(63) Krause, L.; Herbst-Irmer, R.; Sheldrick, G. M.; Stalke, D. Comparison of Silver and Molybdenum Microfocus X-Ray Sources for Single-Crystal Structure Determination. *J. Appl. Crystallogr.* **2015**, *48*, 3−10.
(64) Sheldrick, G. M. *Twinabs*, version 2012/1; Georg-August-Universität Göttingen: Göttingen, Germany, 2012.
(65) Sheldrick, G. M. *Xs*, version 2013/1; Georg-August-Universität Göttingen: Göttingen, Germany, 2013.

https://dx.doi.org/10.1021/acs.organomet.9b00641
Organometallics XXXX, XXX, XXX−XXX

(66) Sheldrick, G. Shelxt - Integrated Space-Group and Crystal-Structure Determination. *Acta Crystallogr., Sect. A: Found. Adv.* **2015**, *71*, 3−8.
(67) Sheldrick, G. Crystal Structure Refinement with SHELXL. *Acta Crystallogr., Sect. C: Struct. Chem.* **2015**, *71*, 3−8.

https://dx.doi.org/10.1021/acs.organomet.9b00641
Organometallics XXXX, XXX, XXX−XXX